Dry slab avalanche shear fracture properties from field measurements

D. M. McClung

Department of Geography, University of British Columbia, Vancouver, British Columbia, Canada

Received 31 January 2005; revised 15 April 2005; accepted 20 June 2005; published 20 October 2005.

[1] Dry slab avalanches release by propagation of shear fractures in a thin, planar weak layer underneath a cohesive, stronger slab. This implies that a balance between shear fracture toughness and the shear fracture stress intensity factor fundamentally determines snow slab stability. Conventionally, fracture toughness is a material property and, for most materials, emphasis is on tensile fracture since most materials fail first in tension. However, for the snow slab, the weak layer fractures first, and field measurements show that the slab material is always stronger than the weak layer. Snow slabs in nature vary with respect to mechanical properties and other characteristics, so the concept of fracture toughness as a material property has no relevance when it is calculated for different avalanches. In this paper, field measurements collected from hundreds of snow slabs are combined with the cohesive crack model to yield estimates for the mode II shear fracture toughness, K_{IIc}. The results suggest that the snow slab has extremely low fracture toughness with variations in nature over more than two orders of magnitude. The nominal weak layer shear strength τ_{Nu} has a power law relationship with respect to the fundamental scaling parameter: the slab thickness, D. Model results also imply that K_{IIc} has power law scaling with respect to D. It is also shown that K_{IIc} follows a log-normal probability density function. This implies a multifractal character by considering the moments, q, of shear fracture toughness scaled with D. Positive multifractal dimensions are suggested for q up to approximately 2.

Citation: McClung, D. M. (2005), Dry slab avalanche shear fracture properties from field measurements, *J. Geophys. Res.*, *110*, F04005, doi:10.1029/2005JF000291.

1. Introduction

[2] Dry slab avalanches release after a shear fracture [shear deformation in both mode II (in plane) and mode III (antiplane) propagates dynamically within a thin weak layer under a cohesive planar slab [*McClung*, 1979, 1981, 2003; *Bažant et al.*, 2003]. (The reader can refer to *Rice* [1968] for the basic mathematical and mechanical background for crack mechanics including the cohesive crack model described below.) *Bažant et al.* [2003] showed that for mode II fracture, D (the slab thickness over the weak layer) is the fundamental scaling or size parameter for the snow slab. They provided a one-dimensional model applicable to fracture initiation which contains two related characteristics of snow slab fracture. First, the fracture process zone is expected to be a significant fraction of the characteristic size D so that the singular crack mechanics pioneered by Griffith must be modified to include a large fracture process zone. Second, a fracture mechanical size effect is implied: weak layer nominal shear strength, τ_{Nu}, should decrease with increasing size D [*Bažant et al.*, 2003] in opposition to increases in τ_{Nu} by densification effects with increasing overburden shear stress as D increases.

[3] Since slab avalanches release by propagating shear fractures, the balance between the stress intensity factor, K_{II}, for mode II loading and slab shear fracture toughness, K_{IIc} determines whether release takes place. In this paper, analyses of K_{IIc} and the major parameters it scales with [*Bažant et al.*, 2003], D and τ_{Nu}, are considered. The results suggest that τ_{Nu} is scale invariant as a function of D. It is suggested,on physical principles, that scale invariance of τ_{Nu} can only apply over a limited range of D. Application of the one-dimensional model of *Bažant et al.* [2003] allows calculation of $K_{IIc}(D)$. The model results combined with avalanche field measurements suggest that $K_{IIc}(D)$ is approximately scale invariant with respect to multiplicative changes in D. This allows estimates of fractal dimensions for three different data sets.

[4] It is also shown that $K_{IIc}(D)$, $\tau_{Nu}(D)$, and D follow log-normal probability density functions (pdf) so that the moments of the pdfs supply some fundamental information about their character. Multifractal analysis of the moments of the pdfs of D for different sets of slab avalanche data with different triggering mechanisms shows that they have virtually the same first moment (Hausdorff) dimension. The multifractal spectra and the fundamental dimensions of K_{IIc}^2, τ_{Nu}, and D (for three data sets of differing triggering mechanisms) are given in relation to the moments in the ranges for which the spectra are nonnegative.

[5] Among the major conclusions of this paper is that even though avalanche shear fracture toughness is fundamental, it cannot be measured prior to slab release. This may have very important implications for avalanche fore-

Copyright 2005 by the American Geophysical Union.
0148-0227/05/2005JF000291$09.00

Table 1. Data Estimated From Dry Slab Avalanche Fracture Lines

Trigger	τ_{Nu} Estimated?	D Estimated?	Number of Avalanches
Mix	yes	yes	191
Skier	no	yes	453
Skier	yes	yes	48
Natural	yes	yes	60

casting. Since the fundamental quantities cannot be measured, avalanche forecasting is a risk-based probabilistic activity with the residual uncertainty due to lack of precision in estimating the needed instability parameters.

2. Description of Data

[6] It was shown [*Bažant et al.*, 2003] that the slab avalanche shear fracture toughness can be estimated as

$$K_{IIc} = \tau_{Nu}(D)\sqrt{\frac{D}{2}}\{O(1)\}, \tag{1}$$

where $O(1)$ represents a scale factor of order 1. Equation (1) holds for large sizes where D is large relative to the fracture process zone size. Below and in Appendix A, this large size limit is extended so that estimates can be made for smaller sizes (D).

[7] The form of equation (1) suggests that K_{IIc} can be estimated entirely from field measurements if τ_{Nu} and D can be found. Below, I describe data taken from fracture line profiles at the crowns of fallen dry slab avalanches to estimate D and τ_{Nu}.

[8] The values of τ_{Nu} are estimated by equating them to down-slope, overburden shear stress, τ_N, applied to the weak layer as

$$\tau_{Nu} \rightarrow \tau_N = \bar{\rho} g D \sin(\psi). \tag{2}$$

The data to estimate τ_{Nu} were taken from the tensile, crown fracture lines from fallen snow slabs including: crown (slab) thickness (D), mean slab density, $\bar{\rho}$, slope angle ψ. In equation (2), g is magnitude of acceleration due to gravity. In cases for which dynamic forces during triggering are possible (explosives and skier loading), this simple relation will be an underestimate [*McClung*, 2003].

[9] It is important that field measurements are used from avalanches since the physical dimensions are very large. It is not possible that the nucleus for fracture initiation is of small size, e.g., on the order of grain size since millions of imperfections of such size are always present in alpine snow packs.

[10] Similarly, it is not possible that the failure strength is homogeneous in a weak layer. This fact has been proven with countless studies starting with that of *Conway and Abrahamson* [1984] and recently by *Landry et al.* [2004] and *Kronholm* [2004]. If weak layers involved in avalanches were homogeneous, such would imply that once loads exceed failure strength in the weak layer, avalanches would initiate everywhere. Dry slab avalanches are rare events and either of these scenarios (microscopic imperfections generating fractures or homogeneous failure strength) would produce many more avalanches than are observed. Therefore it is more likely that dry slab avalanches are generated from imperfections of macroscopic size which may be a significant fraction of a meter [*McClung and Schweizer*, 1999; *Bažant et al.*, 2003]. Since the data used here are from avalanches, the effective sample size in relation to the spatial scale of the weak layer is very large and it should include within it any macroscopic imperfection which was involved in avalanche initiation. It has been known for a long time [e.g., *Perla*, 1977; *Sommerfeld*, 1980; *Jamieson*, 1995] that the shear strength within weak layers, as estimated with shear frame tests, decreases as the spatial size of the sample increases.

[11] I have analyzed four sets of field data from dry slab avalanche fracture lines. The four sets include: measurements of both τ_{Nu} and D for avalanches with a mix of triggers including natural, skier triggered and from explosives, for which the exact percentage of each type of trigger is unknown. The data are derived from *Perla* [1977] and *Stethem and Perla* [1980], data collected over many years by staff of Canadian Mountain Holidays and the personal collections of J. Schweizer, P. Föhn, C. Landry, and B. Wright. Table 1 contains a summary of the data sets.

3. Fracture Toughness Scaling for the Snow Slab

[12] For avalanche situations, the strain and stress conditions within the weak layer are close to simple shear. In simple shear, it is known that alpine snow is a pressure sensitive, dilatant strain-softening material [*McClung*, 1977]. This implies that alpine snow is a quasi-brittle material with a finite sized fracture process zone [*Palmer and Rice*, 1973] which may be on the order of D [*Bažant et al.*, 2003].

[13] It would not be possible to measure shear fracture toughness prior to an avalanche and it would be dangerous to attempt it. Therefore in this paper, K_{IIc} is formulated from a model and field estimates of the parameters in the model are used to calculate it. This is a very common procedure in fracture mechanics for lab samples. For the calculations, the major difference here is that field estimates from avalanches representing large, full-scale sample size are used. Thus field data from slab avalanches observed in nature are used here since they are large size and also they constitute the only realistic data to estimate the nominal shear strength consistent with the presence of macroscopic-scale imperfections. Since field data are used, one cannot expect to achieve the precision of controlled experiments in the laboratory. However, the disadvantage of small samples is minimized since the size of a lab sample required to estimate true fracture toughness would be nearly impossible to achieve [*Bažant et al.*, 2003]. Lab experiments are essential to properly estimate size effect parameters. The appropriate laboratory measurements in shear do not exist and they would be very difficult to obtain.

[14] Figure 1 is a schematic of the loading for snow slab failure as studied by *Bažant et al.* [2003]. It is assumed that strain softening initiates within an imperfection of stress, τ_i, and half length $a_i < a$ (the parameter, a, is crack half length). In Figure 1, the shear stresses are ordered as $\tau_i < \tau_r < \tau_N$, where τ_r is the residual stress after strain softening. In Figure 1, τ_N is nominal shear stress applied to the weak layer which is equated to nominal shear strength at fracture initiation from equation (2).

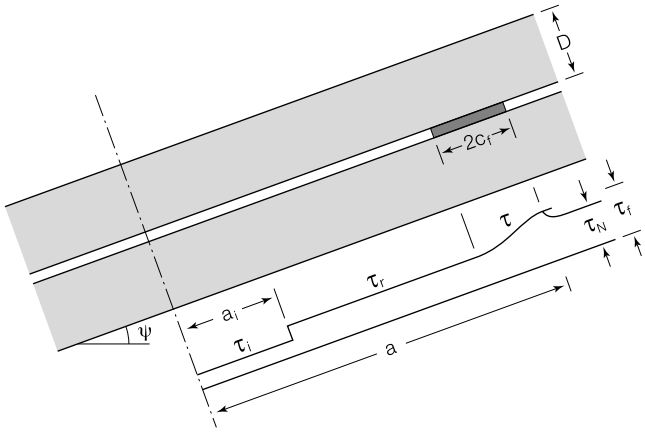

Figure 1. Schematic for snow slab failure. It is suggested that strain softening initiates within an imperfection and spreads under loading to reach a critical condition when $K_{II} \rightarrow K_{IIc}$. In the figure, τ_f is peak failure stress, τ_N is nominal shear stress, τ_r is residual shear stress, τ_i is imperfection shear stress, a_i is imperfection half length, a is crack half length, and $2c_f$ is the fracture process zone size.

[15] *Bažant et al.* [2003] determined the stress intensity factor for mode II loading for the scheme in Figure 1. When fracture is imminent, the replacement: $K_{II} \rightarrow K_{IIc} = \sqrt{E' G_{II}}$ is made with the fracture toughness estimated from nonlinear elastic fracture mechanics [*Bažant et al.*, 2003]. From *Bažant et al.* [2003], E' is the effective modulus for snow slab on a hard base and G_{II} is the fracture energy needed to create a unit shear fracture surface. For the situation in Figure 1, the stress intensity factor is [*Bažant et al.*, 2003]

$$K_{II} = \tau_N \sqrt{D/2}(\alpha_0)\left\{1 - \left(\frac{\tau_r}{\tau_N}\right)\left[1 - \left(\frac{a_i}{a}\right)\left(1 - \frac{\tau_i}{\tau_r}\right)\right]\right\}, \quad D \gg D_0. \tag{3}$$

In equation (3), α_0 is the ratio a/D which is a material constant of order 1, but greater than 1 [*Bažant et al.*, 2003].

[16] Equation (3) is based on the cohesive crack model [*Rice*, 1968] as applied by *Palmer and Rice* [1973] but extended to include the imperfection of half length a_i with $\tau_i < \tau_r$. Equation (3) is derived with the assumption that the material beneath the weak layer is much stiffer than the slab or weak layer which is an approximation. In equation (3), the terms within the curly brackets add to produce of a number of order 1, but less than 1 in typical cases. The product of α_0 and the terms within the curly brackets consists of a number slightly greater than 1 (α_0) and a number less than 1 {.} to give a product of order 1. Assuming the terms inside the curly brackets in equation (3) do not scale with D, or ignoring residual strength in relation to τ_{Nu}, when the fracture toughness is scaled with D, the following relation is obtained [*Bažant et al.*, 2003] when $D \gg D_0$ and $K_{II} \rightarrow K_{IIc}$:

$$K_{IIc} = \sqrt{E' G_{II}} = \tau_{Nu} \sqrt{D/2}\{O(1)\}, \quad D \gg D_0, \tag{4}$$

where $O(1)$ denotes a number of order 1.

[17] Equation (4) applies in the large size limit. An expression to yield values for smaller sizes is derived in Appendix A by Taylor series asymptotic expansion using the equivalent elastic crack concept. This is detailed by *Bažant and Planas* [1998] by relating apparent fracture toughness to true fracture toughness. From Appendix A, the true fracture toughness is estimated as

$$K_{IIc} = \tau_{Nu}(D)\sqrt{D/2}\left(1 + \frac{D_0}{4D}\right). \tag{5}$$

From the one dimensional size effect law of *Bažant et al.* [2003], equation (5) could also be expressed in terms of a horizontal length scale in the weak layer by the replacement (for the expression in parentheses) $D \rightarrow (D_0/2c_f)a_0$ where a_0 is half length of the crack, a minus c_f. The size effect on nominal strength is physically clearer using a horizontal scale a_0 within the weak layer for which shear frame fracture tests show that strength decreases as sample size increases in the thin weak layer. For the avalanche data used to estimate shear strength, the sample size is very large but the effective fracture initiation is predicted to take place within a horizontal scale comparable to D. Thus the large size of the fracture process zone must be taken into account. In this paper, D is chosen for scaling since it is usually known prior to an avalanche.

[18] Field observations consistently show that the ratios of slab length, L, and width, W, to D are such that L/D, $W/D \gg 1$ for fallen snow slabs. *Brown et al.* [1972] presented data from 26 dry slabs to yield a mean value of $W/L = 2.25$. I collected data from 36 dry slabs to yield a mean value for $W/D = 106$. These data suggest that L/D, $W/D \gg 1$ as observed in the field. Field observations consistently show that shear fractures most often initiate at long distances away from the crown, flanks or stauchwall. The one dimensional size effect law used above applies only if the slab length is much larger than the thickness D [*Bažant et al.*, 2003]. Field data and observations consistently suggest that this is the case.

[19] The D_0 parameter is a material constant in the size effect law developed by *Bažant et al.* [2003] which is taken to be 0.1 m for the calculations below. *Bažant and Planas* [1998] suggest that for concrete, D_0 is a multiple of maximum aggregate size, d_a, from about 2 in compression to 20 in tension. For concrete, the volume fraction filled by solids is close to 85%. For alpine snow in avalanches, the volume fraction filled by solids is about 20%. Replacing aggregate size by typical bond size (1 mm) and using the largest value of 20 from concrete in tension gives a rough estimate $D_0 \sim 100 \times$ grain size or about 10 cm. This estimate has to be confirmed by laboratory measurements. It does not seem likely that the number could be as low as 1 cm for snow. It could be larger than 10 cm but probably not 100 cm. I suggest that a fundamental reason to expect finite sized fracture process zones in the quasi-brittle Earth materials (soils, ice, snow) and materials like concrete is that grain sizes are large as opposed to fundamental failure links in brittle materials like glass which may be closer to atomic bond scale. In alpine snow, not only are the failure links (grain size) on the order of mm size, but such links are sparsely concentrated since dry alpine snow in slab avalanches is low density and mostly air. Table 2 contains estimates of K_{IIc} derived from the field estimates outlined in Table 1 and lab estimates of apparent fracture tough-

Table 2. Estimates of K_{IIc} From Slab Avalanche Data and Laboratory Data on Small Homogeneous Samples in Tension (Apparent Fracture Toughness, K_{INu}) From *Schweizer et al.* [2004][a]

Mode	Range, kPa(m)$^{1/2}$	Mean, kPa(m)$^{1/2}$	Source
K_{IIc}	0.2–10	1.79 ± 0.47	60 natural slabs
K_{IIc}	0.16–3	1.32 ± 0.23	48 skier-triggered slabs
K_{IIc}	0.02–13	0.66 ± 0.16	191 slabs with mix of triggers
K_{INu}	0.04–2	0.74 ± 0.10	65 small samples of snow from lab test

[a]The latter do not include size effects expected for a finite fracture process zone. See Appendix A and *Bažant and Planas* [1998] for more information on apparent fracture toughness.

ness, K_{INu} of alpine snow in tension. Apparent fracture toughness [*Bažant and Planas*, 1998] results when toughness is estimated using linear elastic fracture mechanics without accounting for the finite size of the fracture process zone relative to sample size (see Appendix A). The order of magnitude ratios of toughness for slab fractures, ice, concrete and steel are estimated to be: 1:100:1000:100000 (the values are in kPa(m)$^{1/2}$) from *Bažant and Planas* [1998] and *Kirchner et al.* [2000].

[20] The mean values for these data sets are the same order of magnitude (~1 kPa(m)$^{1/2}$) as for alpine snow in tension using small samples and for similar mixed mode (tensile and shear) experiments [*Kirchner et al.*, 2002a, 2002b; *Schweizer et al.*, 2004]. Some of the larger slabs have high-density snow, and high overburden pressures so the higher values at upper range for the slab data may be expected compared to the lab data.

[21] The mean value for apparent tensile fracture toughness K_{INu} from *Schweizer et al.* [2004] ~0.7 kPa(m)$^{1/2}$ for snow (density about 200 kg/m^3) may be compared with the value for solid ice (density 917 kg/m^3) quoted as K_{Ic} = 100 ± 20 kPa(m)$^{1/2}$ [*Petrenko and Whitworth*, 1999] for an increase of about 150 times. *Mellor* [1975] presents data on the Young's modulus of well bonded snow which show that $\sqrt{E}$ increases by a factor of about 100 over the same density range. The values quoted by *Mellor* [1975] are for well bonded snow. *Mellor* [1975] cautions that the Young's modulus for low-cohesion snow can be lower than he lists. Therefore to a first approximation, variations in the Young's modulus with density explain the differences in K_{Ic} between snow and ice.

[22] Since the Young's modulus for ice is virtually independent of temperature (about 5% increase for temperatures from 0°C to −50°C (E. Schulson, personal communication, 2004), any significant variation of K_{Ic} with temperature for snow must reside within the fracture energy G_I. *Nixon and Schulson* [1987] showed that K_{Ic} for ice varies from about 75 kPa(m)$^{1/2}$ at −3°C to 110 kPa(m)$^{1/2}$ at −50°C. *McClung* [2003] showed that dry slab fracture failure temperatures usually range only as low as −15°C in nature. Therefore it may be expected that temperature effects are very small in elastic fracture toughness formulations for the snow slab. However, this may not be so when slow loading is involved in the initiation process and visco-elastic deformation is present [*McClung*, 1996; *Schweizer et al.*, 2004]. Alpine snow may only be treated as completely elastic when deformation rates are high so there is no question that during the initiation of natural releases caused by storm loading there will be important visco-elastic and, therefore, temperature-dependent processes.

[23] Conventional fracture mechanics for engineering materials is sometimes based on the assumption that fracture toughness is a material property. The one-dimensional size effect law of *Bažant et al.* [2003] suggests that D is a simple parameter to characterize shear fracture toughness for a snow slab. For random snow slab data collected in the field, each value is estimated for different slab and weak layer properties, overburden, temperature, size effect and nominal shear strength. This produces scatter in the data and values varying over more than two orders of magnitude. Below, it is shown that these effects combine to give slab nominal shear strength and shear fracture toughness a fractal nature when scaled with D. Thus for the present formulation, shear fracture toughness is characterized only by a given value of D for a given triggering mechanism.

4. Scale Invariance of $K_{IIc}(D)$

[24] Figure 2 shows a log-log plot of $K_{IIc}(D)$ from equation (4) as a function of D for the data set of 191 avalanches with a mix of triggers. A least squares fit gives a line with a slope 1.70 ± 0.05 (95% confidence limits) with R^2 = 0.91 (R is Pearson correlation coefficient). The non-integer slope 1.70 arises primarily from the sum of two terms: approximately 0.5 from the fracture mechanical size effect law (equation (4)) and 1.22 which represents the scale invariant dependence of $\tau_{Nu}(D)$ since a similar plot of τ_{Nu} versus D gives a least squares line with slope 1.22. Table 3 contains similar calculations for the other two data sets.

[25] From the scaling analysis above, Figure 2 suggests that $K_{IIc}(D)$ is approximately invariant under multiplicative

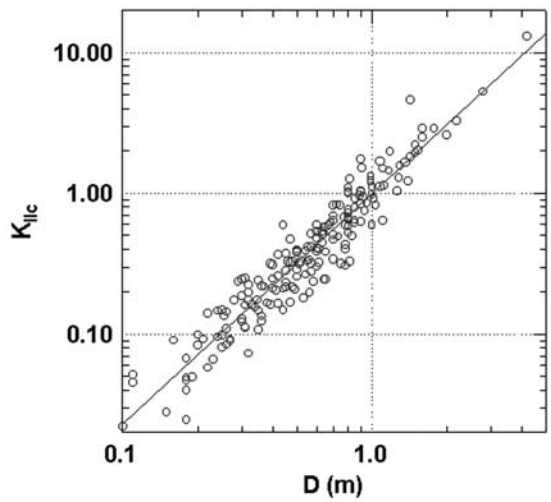

Figure 2. Log-log plot of $K_{IIc}(D)$ in kPa(m)$^{1/2}$ with D for 191 dry slab avalanches with a mix of triggers. The slope of the line is 1.70 ± 0.05 (R^2 = 0.91).

Table 3. Scale Invariant Exponent of $K_{IIc}(D)$ Versus D From Least Squares Regression

Scale Invariant Exponent	Trigger	Number of Slabs	% Variance Explained ($100 \times R^2$)
1.70 ± 0.05	mix	191	91
1.51 ± 0.09	natural	60	81
1.59 ± 0.16	skier	48	90

scale changes of D. See Appendix B for definitions of fractal dimensions and scale invariance. However, the estimates depend upon the scaling relation for $K_{IIc}(D)$ for the stress intensity factor chosen to fit the experimental data. The results are a consequence of the cohesive crack model (Figure 1) and the asymptotic expansion used to derive equation (5). The approximate scale invariance arises from the fact that the mean slab density is nearly independent of D and the range of slope angles is narrow. Field measurements, represented by the data in this paper, show that the same mean slab density can be achieved for small slabs as well as large ones by wind packing and densification by settlement.

[26] I suggest that mode II fracture toughness is of fundamental importance for release of dry slab avalanches. The geometrical self-similar appearance of slab avalanches, with fracture line perpendicular to the bed [*Perla*, 1970; *McClung*, 1981], is related to overcoming shear fracture toughness in order to release avalanches at all scales (imperfection size (small size) to finite size effect (large size)). Once shear fracture takes place, the weak layer or bed friction is reduced to small values. The layered structure (cohesive, strong slab over a thin weak layer) and dynamic effects combine to produce maximum principal stress parallel to the weak layer with the tensile fracture generated perpendicular to the weak layer [*McClung*, 1981]. This effect explains why slab avalanche fracture lines appear the same at any scale (fracture line perpendicular to the weak layer): the release mechanism is tensile fracture caused by dynamic shear fractures propagating up-slope at high speeds.

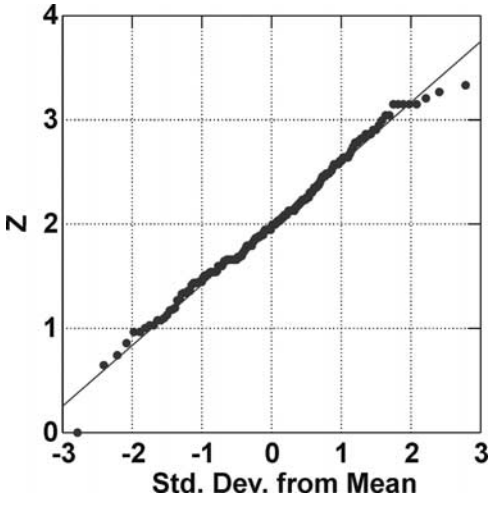

Figure 3a. Probability plot for values of ln(D) from $D = \exp(-Z)$ for 191 slabs with a mix of triggers. The plot suggests that D follows a log-normal probability density function (pdf).

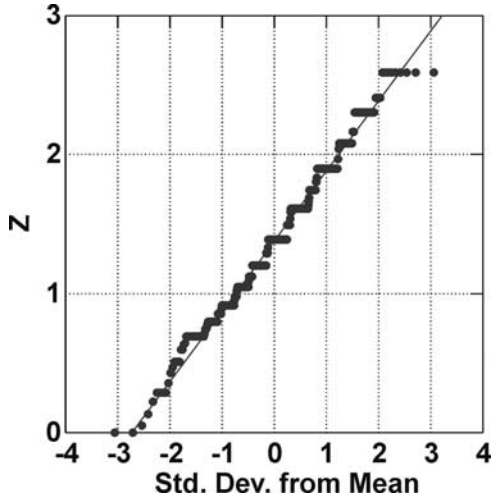

Figure 3b. Probability plot similar to Figure 3a for 446 slabs triggered by skiers.

5. Multifractal Analysis for $K^2_{IIc}(D)$, $\tau_{Nu}(D)$, and D Fitted to pdfs

[27] Both D [*McClung*, 2003] and $\tau_{Nu}(D)$ are log-normally distributed when probability plots are constructed. Since $K^2_{IIc}(D)$ is formed from a product of these, it is also a log-normal variable. This suggests that the moments of $K^2_{IIc}(D)$ characterize it and a multifractal analysis [*Harte*, 2001] is appropriate to estimate multifractal dimensions. Appendix B contains background material relevant to a standard multifractal analysis to determine the fundamental dimensions of $K^2_{IIc}(D)$. Since $K^2_{IIc}(D)$ is proportional to the fracture energy, it is considered here instead of $K_{IIc}(D)$ but the analysis would be similar for the latter.

[28] Consider the analysis of $K^2_{IIc}(D) = E'G_{II}$, $\tau_{Nu}(D)$, and D with the values fitted to a log-normal pdf. The values are scaled such that $0 < (K^2_{IIc(i)}(D))/(K^2_{IIc}(\max)) \leq 1$ by dividing all values by the maximum value of each set. Let the random weight K be defined as $\ln(K) = -Z$ where Z is a random normal variable. For the analysis below, K could represent K^2_{IIc}, τ_{Nu} or D.

[29] Figures 3a and 3b show probability plots for the values of D for the two large data sets introduced above: 191 values from a mix of triggers and 446 values from skier triggering. The probability plots suggest for both data sets, that the values of D follow a log-normal distribution. For Figures 3a and 3b, the skewness and kurtosis are not significant. For the skier triggered slabs, the set was reduced from 453 values to 446 values by eliminating slab sizes below 10 cm. This reduced the kurtosis and skewness to negligible values for Z. Figure 4 contains a probability plot representing $K^2_{IIc}(D)$ and a plot of $\tau_{Nu}(D)$ is similar. The plots imply that K is a positive random variable with a log-normal distribution and a mean equal to b^{-1}. Alternatively, Z is a normal random variable with variance $\sigma^2_{\ln(K)}$ and mean $1/2\sigma^2_{\ln(K)} + \ln(b)$. From Appendix B, equation (B6), the mulifractal dimensions are defined from the moments, q, of K through $\theta^*(q) = -\log_b E[K^q] - 1$.

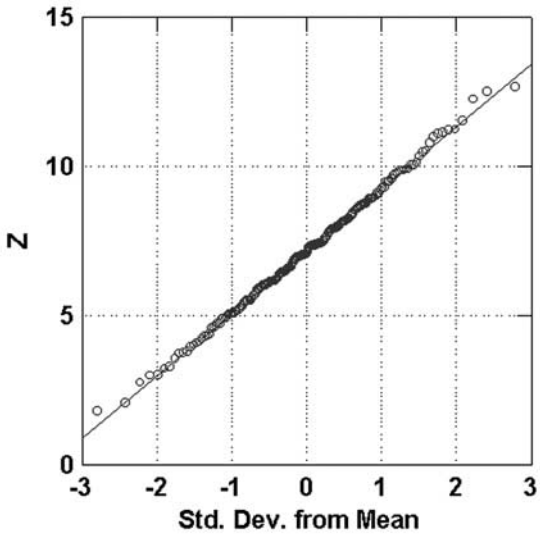

Figure 4. Probability plot for $Z_i = -\ln[K^2_{\mathrm{IIc}(i)}(D)/K^2_{\mathrm{IIc(max)}}]$ for 191 dry slabs with a mix of triggers. The plot suggests that K^2_{IIc} follows a log-normal pdf.

For the log-normal distribution, $\theta^*(q)$ is given easily as, e.g. [*Harte*, 2001]

$$\theta^*(q) = -\Psi q^2 + (\Psi + 1)q - 1, \tag{6}$$

where Ψ is a constant between the limits $0 < \Psi = \{[\sigma^2_{\ln(K)}]/[2\ \ln(b)]\} < 1$ [*Harte*, 2001].

[30] The upper limit on Ψ follows since the measure $\mu([0, 1])$ has an expected value of one only if $\Psi < 1$ [*Harte*, 2001]. Both limits ($0 < \Psi < 1$) are discussed below.

[31] The value of Ψ depends on the scaling of K. Here, the values are scaled to lie between 0 and 1 by dividing all values by the maximum in the set but other choices are available. The numerator, $\sigma^2_{\ln(K)}$, does not depend on the multiplier chosen to scale the measure. However, the value of b^{-1}, the mean value of K, does depend on it. Therefore any dimensions calculated below, which depend on Ψ, also depend on the scaling or normalization to construct the random weight, K.

[32] The Hausdorff dimension is related to the fundamental definition of entropy and it is sometimes called the information dimension. From equation (6) and Appendix B, the Hausdorff dimension is defined from the first moment by *Harte* [2001] as

$$D^*_1 = -bE[K(\log_b K)] = \lim_{q\to 1} \frac{\theta^*(q)}{q-1} = 1 - \Psi. \tag{7}$$

If $\Psi = 1$, $D^*_1 = 0$, then either K is similar to a Dirac delta function with zero variance, or b = 0, which implies that the mean of K is infinite or the mean of $Z \to -\infty$. If $\Psi = 0$, then either the variance of Z is zero or $\ln(b) \to \infty$ and the mean of Z is infinite. Therefore $0 < \Psi < 1$, as suggested above and the values of K^2_{IIc} must be scaled to calculate the multifractal dimensions.

[33] From equation (6) and equation (B7), the Rényi dimensions are given by

$$D^*_q = 1 - q\Psi \qquad q \in R. \tag{8}$$

From equation (8), $D^*_0 = 1$ which corresponds to the zeroth moment of K and is related to the normalization of the measure $\mu[0, 1]$.

[34] From Appendix B (equation (B8)), the multifractal spectrum is derived by solving $(\partial f^*(y))/\partial q = 0$. The values of q on the convex hull of the multifractal spectrum are given by [*Harte*, 2001]

$$q_{\mathrm{crit}} = \frac{1 + \Psi - y}{2\Psi}. \tag{9}$$

Harte [2001] has supplied the spectrum (see equation (B8)) as $f^*(y) = q_{\mathrm{crit}}y - \theta^*(q_{\mathrm{crit}})$:

$$f^*(y) = 1 - \frac{(y - \Psi - 1)^2}{4\Psi}. \tag{10}$$

The spectrum is displayed in Figure 5. The multifractal spectrum takes nonnegative values for $\Psi + 1 - 2\sqrt{\Psi} \le y \le \Psi + 1 + 2\sqrt{\Psi}$.

[35] From equations (8) and (9), the limits on q and D^*_q for which the multifractal spectrum is nonnegative are $-(1/\sqrt{\Psi}) \le q \le (1/\sqrt{\Psi})$ and $1 - \sqrt{\Psi} \le D^*_q \le 1 + \sqrt{\Psi}$. The entropy function, $I_0(y)$, is a nonnegative quadratic defined as [*Harte*, 2001]

$$I_0(y) = 1 - f^*(y) = \frac{(y - \Psi - 1)^2}{4\Psi}, \tag{11}$$

which takes values from 0 to ∞ as y varies from $\Psi + 1$ (at $q = 0$) to $\pm\infty$ ($q \to \mp\infty$). Thus the most probable values of the multifractal dimensions are found near $q = 0$ where the multifractal spectrum is positive. Given the physical limits on which scale invariance is expected for the quantities considered in this paper (Figure B1), it is suggested that portions of the multifractal spectrum for which $f^*(y)$ is negative will not have any physical significance. Thus D^*_q should be confined to the limits $1 \pm \sqrt{\Psi}$.

[36] Table 4 contains the Hausdorff dimensions and the ranges of q and D^*_q for variables which follow log-normal pdfs. The results show that the multifractal dimensions are nearly the same for D independent of the triggering mechanism and the Hausdorff dimension of τ_{Nu} is nearly the same as for D. Figure 6 shows the multifractal dimensions D^*_q versus q over the nonnegative portion of the multifractal spectrum for the probability plot of $K^2_{\mathrm{IIc}}(D)$ similar to Figure 4.

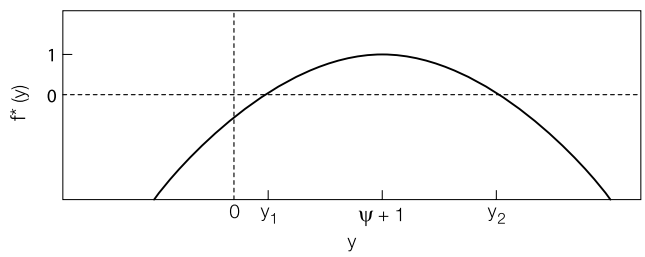

Figure 5. Multifractal spectrum for a log-normal variable after *Harte* [2001]. The spectrum is applied to $\tau_N(D)$, $K^2_{\mathrm{IIc}}(D)$, and D since they all follow a log-normal pdf. In the figure, $f^*(y)$ is nonnegative for $\Psi + 1 - 2\sqrt{\Psi} \le y \le \Psi + 1 + 2\sqrt{\Psi}$ or $y_1 \le y \le y_2$.

Table 4. Hausdorff Dimensions, D_1^*, and Ranges of q and D_q^* for Nonnegative Multifractal Spectra for Variables Which Follow Log-Normal Probability Density Functions With Ψ Scaled to be in the Range 0–1

Variable	Trigger	Ψ	D_1^*	Range of q	Range of D_q^*	Number of Slabs
$K_{IIc}{}^2(D)$	mix	0.51	0.49	±1.40	0.29–1.71	191
$\tau_N(D)$	mix	0.15	0.85	±2.58	0.61–1.39	191
D	mix	0.10	0.90	±3.16	0.68–1.32	191
D	skier	0.10	0.90	±3.16	0.68–1.32	446
D	natural	0.17	0.83	±2.40	0.83–1.17	60

[37] For $K_{IIc}^2(D)$ in Table 4, negative dimensions are predicted for $q > 1.96$. However, the values in Table 4 are heavily influenced by the normalization scaling of the measure. Valid comparisons of dimensions in Table 4 are only reasonable for the values corresponding to the measure D since they are all of the same units. If the values are constructed by dividing by the sum of all the values similar to the procedure above, the values of ψ for the measures are

$$K_{IIc}^2(D)\{\Psi = 0.41\}, \quad \tau_{Nu}(D)\{\Psi = 0.07\}, \quad D\{\Psi = 0.03\}, \quad D\{\Psi = 0.02\}, \quad D\{\Psi = 0.04\},$$

in the same order as in Table 4. Thus the predicted ranges of q and D_q^* and the values of the Hausdorff dimensions can change substantially depending on how the data are scaled.

6. Summary and Discussion

[38] Slab avalanche shear fracture toughness is suggested to vary by nearly three orders of magnitude in nature mainly due to natural variations in nominal shear strength. The mean value from the investigation here is on the order of $\sim$1 kPa(m)$^{1/2}$ which is about 1% of the toughness value for the matrix material ice in tension. The values are extremely low compared to ice, concrete and steel. In the context of avalanche release by propagating shear fractures, shear strength has no meaning by itself but it is a very important component of fracture toughness [*Bažant et al.*, 2003]. Instead of low strength, a more correct description is that the fracture toughness of snow is extremely low. On the basis of shear strength data, it is expected to be the lowest of any of the common Earth materials (snow, soils, rock ice). This is a fundamental reason why snow avalanches are of much higher frequency than landslides, debris, rock or large ice avalanches.

[39] It is highly unlikely that classical linear elastic fracture mechanics (also called singular crack mechanics) as developed by Griffith applies either to alpine snow or avalanche fracture problems. Alpine snow is a strain-softening, quasi-brittle material composed of millimeter sized grains with a typical volume fraction filled by solids of 20% for avalanche problems. Griffith fracture mechanics applies when the fracture process zone is insignificant in relation to sample size [*Bažant and Planas*, 1998]. The scaling in this paper and *Bažant et al.* [2003] suggests that quasi-brittle fracture mechanics taking into account a finite sized fracture process zone must be used to formulate fracture toughness both in the laboratory and for the avalanche problem in the field since the fracture process zone can be a significant fraction of D.

[40] The field data suggest that τ_{Nu} is scale invariant with respect to D according to the mathematical definition of scale invariance (equation (B1)) in this paper as defined by *Jensen* [1998]. This is due to different combinations of mean slab density, slab depth and slope angle. Thus τ_{Nu} is a power law function of D so no characteristic scale appears under a multiplicative change in D.

[41] On the basis of scaling arguments presented by *Bažant et al.* [2003], $K_{IIc}(D)$ or $K_{IIc}^2(D)$ is expected to be approximately invariant with respect to multiplicative scale changes in slab thickness, D. The expected range of invariance is between imperfection size generating fractures to very large sizes depending on bonding and densification. The approximate scale invariance is not trivial. It arises from proportionality to nominal shear strength in the expression derived from the stress intensity factor and the results are consistent for three data sets. Any scale invariance suggested for $K_{IIc}(D)$ depends on a model. Thus it is much more tentative than scale invariance suggested for $\tau_{Nu}(D)$. The one dimensional approximation for the size effect law of *Bažant et al.* [2003] requires extension if estimates are to be made for slab thicknesses, D, which are very large.

[42] The geometrical similarity for the appearance of slab avalanche fracture lines arises from persistent observations and measurements that the fracture line is perpendicular to the weak layer or failure surface at the base of the slab. This is likely due to tensile fracture at the arrival of a dynamic propagating shear fracture [*McClung*, 1981]. The appearance suggests that the fracture mechanism is independent of scale, D, but such cannot be proven by the data and analysis in this paper. However, field observations of dry avalanche release show that the mechanism is the same regardless of

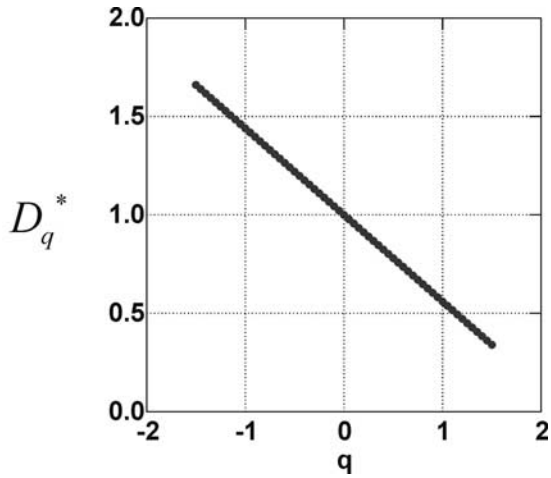

Figure 6. Multifractal dimensions D_q^* for $K_{IIc}^2(D)$ in the range over which the multifractal spectrum is nonnegative: $-1.4 \leq q \leq 1.4$.

scale D just as described above. *Hergarten* [2002] gave an heuristic definition of a fractal: an object that looks the same at all scales. This fits for avalanche fracture lines in spite of the fact that they are Euclidean consisting of a line. However, a fractal dimension cannot be assigned to a set of avalanche fracture lines.

[43] All the avalanche data sets suggest that D follows a log-normal distribution which implies that the sets of D are not scale invariant [*McClung*, 2003]. Since $K_{\mathrm{II}c}(D)$ is built from the product of $\sqrt{D}$ and $\tau_N(D)$, it is also a log-normal variable. *Harte* [2001] provides the method for a multifractal analysis of a log-normal variable which is applied to the data sets in this paper. The multifractal analysis shows that the fundamental dimensions over which the mutlifractal spectrum is positive depend on the divisor used to scale the data. However, the dimensions of D are nearly the same suggesting they are independent of triggering mechanism for the same divisor. More importantly, the analysis suggests that a complete mathematical description of shear fracture properties will not be provided by a single fractal dimension.

[44] The fracture toughness squared is proportional to the fracture energy. The scale invariant exponents for $K^2_{\mathrm{II}c}(D)$ include: 3.4 (mix of triggers); 3.2 (skier triggers); and 3.0 (natural triggers). *Korvin* [1992, p. 204] provides an extensive list of fractal dimensions for fragmented materials from earth and extra terrestrial sources in the range 1.4–3.6. *Korvin* [1992] suggests that scale invariance of the fragmentation mechanism is linked to preexisting zones or planes of weakness which can be found on all scales. In the fragmentation process, it is suggested [*Korvin*, 1992] that fracture at a macroscopic scale is a consequence of accumulation of fractures at lesser scales which is similar to the damage process for quasi-brittle materials [*Bažant and Planas*, 1998]. Avalanche energy exponents are within the ranges of fractal dimensions of fragmented earth materials from other studies but it is too early to link the processes to fragmentation theories. Lab data by *Schweizer et al.* [2004] for 65 samples of alpine snow suggest that K^2_{Ic} (tensile fracture toughness squared) is approximately scale invariant with snow density and an approximate exponent of 4.

[45] For discussion, it is suggested that even though $K_{\mathrm{II}c}$ is fundamentally important for the snow slab, it cannot be measured in situ so that the scaling argument is the only known way of estimating it. Since $K_{\mathrm{II}c}$ cannot be measured easily, there are profound implications for avalanche prediction, particularly for backcountry travel which accounts for most avalanche fatalities in North America and Europe [*McClung and Schaerer*, 1993]. I suggest that that macroscopic imperfections on the order of 10 cm serve as stress concentrators to initiate avalanches which casts doubt on reliability of some slope stability tests (see *McClung and Schaerer* [1993] for a summary of the tests) as indicators of potential avalanche danger. *Sommerfeld and Gubler* [1983] estimated fracture areas of 10 cm to 1 m radius from the frequency spectra of low-frequency acoustic emissions which provides additional support to the minimum imperfection size argument in this paper. It would be rare for small area tests to include such an imperfection. The suggestion that some small area tests can lack critical information casts avalanche forecasting into the realm of risk and probability [*McClung*, 2002a, 2002b].

[46] The difficulty and danger in measuring shear fracture toughness in the field also places limitations on any conclusions in this paper. Even though the estimates are derived from field measurements, it must be considered that there are no in situ measurements to completely validate the results. Such measurements would be very difficult to obtain. The full solution to this problem will require careful small-scale lab experiments coupled with field validation.

Appendix A: Relating True and Apparent Fracture Toughness for Mode II

[47] When fracture toughness is calculated from a model assuming linear elastic fracture mechanics (LEFM) for a material which has a finite sized fracture process zone, as expected for alpine snow, the result gives an apparent fracture toughness. The concept of fracture toughness (called true fracture toughness) is that it applies to brittle fracture with LEFM assumed to apply. For the size effect law of *Bažant et al.* [2003] in this paper, it is appropriate to assume that LEFM applies in the limit of large (D) size. However, simple methods are available to approximate fracture toughness for smaller sizes. One of these is to relate apparent fracture toughness to true fracture toughness for quasi-brittle materials as shown by *Bažant and Planas* [1998] using the equivalent elastic crack concept in their book. The development here follows the logic of *Bažant and Planas* [1998, pp. 108–111], but it is slightly modified as a result of a personal communication with Z. P. Bažant (2004).

[48] From *Bažant and Planas* [1998], the true fracture toughness is defined as

$$K_{\mathrm{II}c} = \tau_{\mathrm{Nu}}\sqrt{D}k(\alpha_{ec}), \tag{A1}$$

where the equivalent crack length is defined as $a_{ec} = a_0 + \Delta a_{ec}$ with a_0 as initial crack length and Δa_{ec} as extension. For the critical crack length, $\alpha_{ec} = \alpha_0 + \Delta a_{ec}/D$. It is shown by *Bažant and Planas* [1998] that $\Delta a_{ec} \approx c_f \ll D$ so that a two term Taylor series expansion gives

$$k(\alpha_{ec}) \approx k(\alpha_0) + k'(\alpha_0)\frac{c_f}{D}. \tag{A2}$$

From *Bažant and Planas* [1998], the apparent fracture toughness is given by

$$K_{\mathrm{IINu}} = \tau_{\mathrm{Nu}}\sqrt{D}k(\alpha_0). \tag{A3}$$

From equations (A1)–(A3), an expression relating true and apparent fracture toughness results:

$$K_{\mathrm{II}c} = K_{\mathrm{IINu}}\left(1 + \frac{c_f}{D}\frac{k'(\alpha_0)}{k(\alpha_0)}\right). \tag{A4}$$

From *Bažant and Planas* [1998], an intrinsic, characteristic size D_c is defined as

$$\frac{1}{D_c} = \left[\frac{\partial \ln K^2_{\mathrm{II}}(\alpha)}{\partial a}\right]_{a=a_0} = \left[\frac{\partial \ln k^2(\alpha)}{\partial a}\right]_{a=a_0}, \tag{A5}$$

and the asymptotic deviation from LEFM is expressed as

$$K_{IIc} = K_{IINu}\left(1 + \frac{c_f}{2D_c}\right). \quad \text{(A6)}$$

Equations (A4) and (A6) are similar to asymptotic equations of *Bažant and Planas* [1998] but they have broader applicability in terms of asymptotic behavior as $D_c \rightarrow 0$. For mode I, the same formalism will apply but, of course, the size effect law has a different form. From equation (A5), $1/D_c = 1/a_0$, and from the one-dimensional size effect law of *Bažant et al.* [2003], $c_f/a_0 = D_0/2D$ and (A6) becomes for the one-dimensional size effect law

$$K_{IIc} = \tau_{Nu}\sqrt{D/2}\left(1 + \frac{D_0}{4D}\right). \quad \text{(A7)}$$

Appendix B: Fractal and Multifractal Definitions Applied to the Snow Slab

B1. Fractal Definitions

[49] There is no general agreement among scientists about definitions applicable to fractal analysis. In this section, I will introduce some definitions containing the general features which most authors use. I will restrict the definitions to those for which the scale is D, the fundamental scaling parameter for the snow slab [*Bažant et al.*, 2003; *McClung*, 2003].

B1.1. Scale Invariance

[50] A physical measure M, such as τ_{Nu}, is scale invariant with respect to multiplicative change of scale if [e.g., *Jensen*, 1998]

$$M(\lambda D) = \lambda^{\alpha} M(D) \quad \text{(B1)}$$

over a range of values for D, where λ and α are constants. In nature, scale invariance (if observed) is followed only over a limited scale range (D). Figure B1 shows a schematic for $\tau_{Nu}(D)$ which is suggested by least squares lines fit through the data in this paper. At some large scale for D, I suggest that scale invariance will break down. Occurrence of largest sizes is also related to the energy supplied by the triggering mechanism and densification due to creep and bonding as time proceeds [*McClung*, 2003]. For example, *McClung* [2003] shows that skier triggered snow slabs for $D > 1$ m are quite rare but such large slabs may be more common if explosives are supplied. At the lowest scale extreme, it is not possible to generate slab avalanches where the scale is on the order of grain size, so that one cannot expect the scaling relation to hold when D is on the order of grain size (1 mm). I suggest that the small-scale extreme is related to macroscopic imperfections perhaps of the order of 100 $\times$ grain size or larger which serve as stress concentrators in the weak layer to initiate fracture.

B1.2. Fractals

[51] A set of objects (for example slab avalanche fracture depths: D) displays scale invariance (or self-similarity) if a ranked set of numbers scales with D:

$$N(D' > D) \sim D^{-n}, \quad \text{(B2)}$$

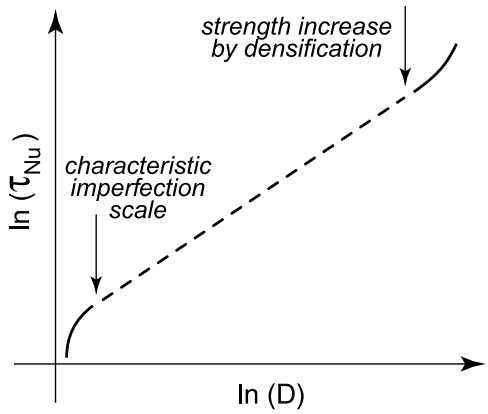

Figure B1. Schematic for possible range of scale invariance for τ_{Nu} versus D. If scale invariance is followed, it will only be within a limited range of sizes (dashed line) for this physical quantity.

where $N(D' > D)$ is the number of objects with characteristic dimension larger than D. In general, the value of n is not an integer so the term fractal is used [*Mandelbrot*, 1967] to describe a fractional dimension, n. For the slab avalanche, an individual fracture line is Euclidian: it constitutes a one-dimensional line. However, it may be possible that a distribution of fracture line sizes is scale invariant if such a relation is followed. Again, if scale invariance is followed, it is expected only over a limited range of D.

[52] A formulation similar to equation (B2) can be used with probability of exceedance replacing $N(D' > D)$ since both are calculated from the ranks of a data set consisting of a discrete set of values of D. Thus in equation (B2), $N(D' > D)$ is related, but not equivalent, to probability of exceedance, $P(D' > D)$. It may be also represented by a normalized cumulative distribution of sizes [*Hergarten*, 2002]:

$$P(D' > D) \sim D^{-n}. \quad \text{(B3)}$$

The relationship in expression (B3) does not hold over any significant range of D for data sets with different triggering mechanisms due partly to finite size effects limiting the largest slab for a given triggering energy input. *Korvin* [1992] suggests that linearity on a double logarithmic plot should extend over at least two or three orders of magnitude in size in order to claim scale invariance. This is not true for snow slabs: finite size effects (depending on triggering energy) can limit [*McClung*, 2003] the largest sizes (e.g., several meters) and invariance cannot hold on the scale of single bonds or imperfections (millimeters to tens of centimeters, respectively). Sizes of interest range from about 10 cm in thickness to several meters. Thus only about two orders of magnitude variations in D are normally observed. Also, since D follows a log-normal distribution, it is not possible that a power law function, as in equation (B3), is followed by the exceedance probabilities.

B1.3. Size Effects

[53] There are two important size effects for avalanche shear fracture properties: finite size effect (or upper limit) on a physical quantity (e.g., D) and a fracture finite size effect

predicted for shear strength whereby shear strength decreases with increasing sample size [*Bažant et al.*, 2003].

[54] The finite size effects (upper limit) can modify the values of a physical measure or scalar by producing an upper bound on scale invariance. For example, the values of D are limited by the energy supplied by skiers triggering avalanches [*McClung*, 2003]. Another reason for an upper limit to scale invariance for $\tau_{Nu}(D)$ (see Figure B1) is that densification, bonding and metamorphism can ultimately produce a homogeneous structure instead of the thin weak layer required for mode II propagation to produce slab avalanches.

[55] Since slab avalanches initiate by propagating shear fractures there is a size effect related to fracture mechanics scaling. Of major importance is that alpine snow is a strain-softening, quasi-brittle material [*Bažant et al.*, 2003; *McClung*, 1977, 1979, 1981, 2003] so that fracture initiation implies a finite sized fracture process zone which can be a significant fraction of D. The implication is that classical Griffith linear elastic fracture mechanics, which is constructed for infinitesimal fracture process zones in relation to sample size, will not apply to the snow slab. The large fracture process zone implies that a fracture mechanical size effect is contained in snow slab stress intensity factor [*Bažant et al.*, 2003] so that $\tau_{Nu} \sim D^{-1/2}$ for large sizes when the large size of the fracture process zone is taken into account. It is shown above and by *Bažant et al.* [2003] that nominal shear strength also increases with D by densification and overburden effects to yield a scale invariant character for $\tau_{Nu}(D)$.

B1.4. Multifractals

[56] The term multifractals is an extension of the definition of self-similarity (or scale invariance) from fractal sets to physical measures. The concept of a fractal is intended to prescribe a unique fractal dimension to a set. Multifractals are intended to describe the distribution of a physical scalar quantity (e.g., K_{IIc} or τ_{Nu}) in terms of a parameter (such as D in this case) when more than one fractal dimension is appropriate. In this paper, dimensions are estimated from the moments of shear fracture properties for the probability density function (pdf) using the data as a continuous set of values fitted to a pdf. The analysis suggests that a complete description of slab avalanche shear fracture properties will require multifractal analysis.

B2. Multifractal Method to Characterize the Distribution of Shear Fracture Properties

[57] There are several methods to display the dimensional properties of a measure [*Evertsz and Mandelbrot*, 1992; *Harte*, 2001]. In this paper, a method is used analogous to a random cascade process by taking the values as a continuous set fitted to a pdf [*Harte*, 2001]. For the method, a random weight, K (representing D, τ_{Nu} or K^2_{IIc}) is constructed in the form of a continuous probability density function. The construction of K to represent a continuous set of values is described below since the mathematical relations are used above.

[58] The values of D and $\tau_N(D)$ follow a log-normal pdf [*McClung*, 2003]. Similar dependence is displayed by $K_{IIc}(D)$ if the cohesive crack model is assumed to calculate the values. It is then appropriate to investigate the moments of these pdfs by envisioning values as a continuous set instead of a discrete set values. If a set of values for a parameter follow a pdf then the moments of the pdf completely describe the set. Most fractal sets in Nature are random fractal sets [*Evertsz and Mandelbrot*, 1992]. In such cases, it is often true that a measure constructed from data follows a probability density function. *Bažant et al.* [2003] and *McClung* [2003] have suggested that K_{IIc} (or K^2_{IIc}) can be scaled with D as suggested by fracture mechanical size effect scaling. *McClung* [2003] shows that $K^2_{IIc}(D)$ and $\tau_{Nu}(D)$ follow a log-normal probability density function. This suggests an analysis using the log-normal probability function for D, $\tau_{Nu}(D)$, and $K^2_{IIc}(D)$.

[59] For construction of a multifractal spectrum, let $K(D)$ be a nonnegative random dummy variable with mean $E(K) = b^{-1}$ where K is represented by a measure, μ, on the interval [0, 1]. A measure, μ, may then be defined as

$$\mu \stackrel{\Delta}{=} K(D), \tag{B4}$$

where $\stackrel{\Delta}{=}$ is used to denote equality of probability density functions and where $0 < K_i(D)/K_{max} \leq 1$ (i.e., the set of values of K_i) are scaled by dividing all values by the maximum value in the set).

[60] Here, a random set of values or weights, K_i, is fitted to a probability density function which is then assumed to take a continuous (infinite) set of values denoted by μ. Thus the positive random variable, K, is represented by a probability density function. The multifractal spectrum may be related to the moments of order q for K by the MKP (Mandelbrot-Kahane-Peyrière) function $\chi_b(q)$:

$$\chi_b(q) = \log_b E[K^q] + 1. \tag{B5}$$

See *Holley and Waymire* [1992] and *Harte* [2001] for more details.

[61] The fundamental dimensions of the multifractal spectrum may be calculated from [*Harte*, 2001]

$$\theta^*(q) = -\log_b E[K^q] - 1. \tag{B6}$$

The Rényi multifractal dimensions represent the fundamental dimensions in relation to the moment order q and are given by [*Harte*, 2001]

$$D^*_q = \frac{\theta^*(q)}{q-1}. \tag{B7}$$

The Hausdorff dimension is the fundamental dimension for moment order $q = 1$. For the conditions assumed above [*Harte*, 2001; *Holley and Waymire*, 1992; *Kahane and Peyrière*, 1976], the Hausdorff dimension is given by $D^*_1 = -bE[K \log_b K] = \lim_{q\to 1}(\theta^*(q)/q - 1)$. It is analogous to the fundamental definition of entropy and information.

[62] Given the assumption that K is defined by a random measure $\mu(0, 1)$, the multifractal spectrum [*Harte*, 2001] may be calculated as

$$f^*(y) = \inf_q \{qy - \theta^*(q)\}, \qquad y \in R, \tag{B8}$$

where inf denotes infimum and $f^*(y)$ is a continuous, closed convex hull of values. Since random sets are dealt with in

this paper, it can be expected that the limits $-\infty < f^*(y) \leq 1$ will apply so the multifractal spectrum can take negative values [*Harte*, 2001]. The interpretation of the Hausdorff dimension described above will only apply for values in which $f^*(y) > 0$ and physical meaning is unclear when $f^*(y) < 0$ [*Harte*, 2001]. The advantage of fitting data to a pdf is that weighting is accounted for. The disadvantage is that a discrete set of values is idealized as a continuous function represented by a pdf which might be taken to apply outside the physical limits of the range of the data. Thus information about finite size effects may not be displayed.

[63] **Acknowledgments.** This research was funded by Canadian Mountain Holidays, the Natural Sciences and Engineering Research Council of Canada, and the University of British Columbia. Data were provided by the mountain guides of Canadian Mountain Holidays, Ron Perla, Juerg Schweizer, Paul Föhn, Chris Landry, Blyth Wright, and Chris Stethem. I am extremely grateful for all these sources of support and data.

References

Bažant, Z. P., and J. Planas (1998), *Fracture and Size Effect in Concrete and Other Quasi-brittle Materials*, 616 pp., CRC Press, Boca Raton, Fla.

Bažant, Z. P., G. Zi, and D. McClung (2003), Size effect law and fracture mechanics of the triggering of dry snow slab avalanches, *J. Geophys. Res.*, *108*(B2), 2119, doi:10.1029/2002JB001884.

Brown, C. B., R. J. Evans, and E. R. LaChapelle (1972), Slab avalanching and the state of stress in fallen snow, *J. Geophys. Res.*, *77*, 4570–4580.

Conway, H., and J. Abrahamson (1984), Snow stability index, *J. Glaciol.*, *30*, 321–327.

Evertsz, C., and B. Mandelbrot (1992), Multifractal measures, in *Chaos and Fractals*, edited by H.-O. Peitgen, H. Jürgens, and D. Saupe, pp. 921–953, Springer, New York.

Harte, D. (2001), *Multifractals: Theory and Applications*, 248 pp., CRC Press, Boca Raton, Fla.

Hergarten, S. (2002), *Self-Organized Criticality in Earth Systems*, 272 pp., Springer, New York.

Holley, R., and E. C. Waymire (1992), Multifractal dimensions and scaling exponents for strongly bounded random cascades, *Ann. Appl. Probab.*, *2*, 819–845.

Jamieson, J. B. (1995), Avalanche prediction for persistent snow slabs, Ph.D. thesis, 258 pp., Univ. of Calgary, Canada.

Jensen, H. J. (1998), *Self-Organized Criticality*, *Cambridge Lecture Notes Phys.*, vol. 10, 153 pp., Cambridge Univ. Press, New York.

Kahane, J. P., and J. Peyrière (1976), Sur certaines martingales de Benoit Mandelbrot, *Adv. Math.*, *22*, 131–145.

Kirchner, H. O. K., G. Michot, and T. Suzuki (2000), Fracture toughness of snow in tension, *Philos. Mag. A*, *80*, 1265–1272.

Kirchner, H. O. K., G. Michot, and J. Schweizer (2002a), Fracture toughness of snow in shear and tension, *Scr. Mater.*, *46*, 425–429.

Kirchner, H. O. K., G. Michot, and J. Schweizer (2002b), Fracture toughness of snow in shear under friction, *Phys. Rev. E.*, *66*, 1–3.

Korvin, G. (1992), *Fractal Models in the Earth Sciences*, 396 pp., Elsevier, New York.

Kronholm, K. (2004), Spatial variability of snow mechanical properties with regard to avalanche formation, Ph.D. thesis, 187 pp., Swiss Federal Inst. of Technol., Zurich, Switzerland.

Landry, C., K. W. Birkeland, K. Hansen, J. J. Borkowski, R. L. Brown, and R. Aspinall (2004), Variations in snow strength and stability on uniform slopes, *Cold Reg. Sci. Technol.*, *39*, 205–218.

Mandelbrot, B. (1967), How long is the coast of Britain? Statistical self-similarity and fractional dimension, *Science*, *156*, 636–638.

McClung, D. M. (1977), Direct simple shear tests on snow and their relation to slab avalanche formation, *J. Glaciol.*, *19*, 101–109.

McClung, D. M. (1979), Shear fracture precipitated by strain-softening as a mechanism of dry slab avalanche release, *J. Geophys. Res.*, *84*, 3519–3526.

McClung, D. M. (1981), Fracture mechanical models of dry slab avalanche release, *J. Geophys. Res.*, *86*, 10,783–10,790.

McClung, D. M. (1996), The effects of temperature on fracture in dry slab avalanche release, *J. Geophys. Res.*, *101*, 21,907–21,920.

McClung, D. M. (2002a), The elements of applied avalanche forecasting part I: The human issues, *Nat. Hazards*, *26*, 111–129.

McClung, D. M. (2002b), The elements of applied avalanche forecasting part II: The physical issues and the rules of applied avalanche forecasting, *Nat. Hazards*, *26*, 131–146.

McClung, D. M. (2003), Size scaling for dry snow slab release, *J. Geophys. Res.*, *108*(B10), 2465, doi:10.1029/2002JB002298.

McClung, D., and P. Schaerer (1993), *The Avalanche Handbook*, 271 pp., Mountaineers, Seattle, Wash.

McClung, D. M., and J. Schweizer (1999), Skier triggering, snow temperatures and the stability index for dry-slab avalanche initiation, *J. Glaciol.*, *45*, 190–200.

Mellor, M. (1975), A review of basic snow mechanics, *IASH Publ.*, *114*, 251–291.

Nixon, W. A., and E. M. Schulson (1987), A micromechanical view of the fracture toughness of ice, *J. Phys. Colloque C1*, *48*, 313–319.

Palmer, A. C., and J. R. Rice (1973), The growth of slip surfaces in the progressive failure of over-consolidated clay, *Proc. R. Soc. London, Ser. A*, *332*, 527–548.

Perla, R. (1970), The slab avalanche, Ph.D. thesis, 101 pp., Dep. of Meteorol., Univ. of Utah, Salt Lake City.

Perla, R. (1977), Slab avalanche measurements, *Can. Geotech. J.*, *14*, 206–213.

Petrenko, V. F., and R. W. Whitworth (1999), *Physics of Ice*, 373 pp., Oxford Univ. Press, New York.

Rice, J. R. (1968), Mathematical analysis in the mechanics of fracture, in *Fracture: An Advanced Treatise*, vol. 2, *Mathematical Fundamentals*, edited by H. Liebowitz, pp. 192–311, Elsevier, New York.

Schweizer, J., G. Michot, and H. O. K. Kirchner (2004), On the fracture toughness of snow, *Ann. Glaciol.*, *38*, 1–8.

Sommerfeld, R. A. (1980), Statistical models of snow strength, *J. Glaciol.*, *26*, 217–223.

Sommerfeld, R. A., and H. Gubler (1983), Snow avalanches and acoustic emissions, *Ann. Glaciol.*, *4*, 271–276.

Stethem, C., and R. Perla (1980), Snow-slab studies at Whister Mountain, British Columbia, Canada, *J. Glaciol.*, *26*, 85–91.

D. M. McClung, Department of Geography, University of British Columbia, 1984 West Mall, Vancouver, BC, Canada V6T 1Z2. (mcclung@geog.ubc.ca)